2

Giant (GMR) and Tunnel (TMR) Magnetoresistance Sensors: From Phenomena to Applications

Càndid Reig and María-Dolores Cubells-Beltrán

CONTENTS

ABSTRACT Solid state magnetic sensors have inherent characteristics that make them potential candidates in a huge range of applications regarding magnetic field sensing. We mention their high level of integration with electronics, their low weight, low cost, and wide bandwidth, among others. Hall effect devices and magnetoresistance sensors are excellent examples. Giant magnetoresistance (GMR) and tunneling magnetoresistance (TMR) sensors, while maintaining these advantages, have demonstrated better performance figures regarding sensitivity and signal-to-noise ratio (SNR). In this way, GMR/TMR sensors have been considered in scenarios requiring sub-nT measurements, with demonstrated success. In this chapter, we will present the fundamental basis of GMR/TMR and we will describe the state-of-the-art use of GMR/TMR sensors.

2.1 Introduction

The giant magnetoresistance (GMR) effect was first described in 1988 by A. Fert (Baibich et al. 1988) and then in 1989 by P. Grunberg (Binasch et al. 1989). In 2007, both were awarded the Nobel Prize in Physics for their contributions (Thompson 2008). Basically, the GMR effect is a significant change in its resistance with an external field at room temperature. It is observed in multilayered structures with ferromagnetic layers separated by a non-magnetic spacer due to the relative orientation of the magnetization vectors.

Initially, GMR structures were used as sensing elements in the read heads of hard drives. In these applications, the magnetoresistance (MR) level shifted, with the influence of the magnetic field generated by the magnetically stored bits, between two limit states: maximum and minimum resistance, as described by

$$MR = \frac{R^{\uparrow\downarrow} - R^{\uparrow\uparrow}}{R^{\uparrow\uparrow}}$$

where:

MR is the so-called magnetoresistance level
$R^{\uparrow\downarrow}$ is the (maximum) resistance in the anti-parallel state
$R^{\uparrow\uparrow}$ is the (minimum) resistance in the parallel state

Nowadays, these multilayered structures can be engineered in such a way that the quiescent state of the structure is obtained with layers having their magnetic moments in a crossed-axis (orthogonal) configuration by means of a particular deposition process or by the application of an external magnetic biasing. In this way, the transfer curve of the device is notably smoothed, and the quiescent working point is placed in a medium state, thereby providing a useful quasi-linear region that can be utilized for analog magnetic sensing applications.

2.2 Structures and Phenomena

GMR phenomena were initially reported on Fe/Cr thin multilayers (Baibich et al. 1988; Binasch et al. 1989). It was demonstrated that the electric current in a magnetic multilayer consisting of a sequence of thin magnetic layers separated by equally thin non-magnetic metallic layers is strongly influenced by the relative orientation of the magnetizations of the magnetic layers (about 50% at 4.2 K). The cause of this giant variation in the resistance is attributed to the scattering of the electrons at the layers' interfaces. In this way, any structure with metal–magnetic interfaces is a candidate to display GMR. Since then, a huge effort has been made to find structures that enhance this effect (MR levels at room temperature above 200% are achieved in modern GMR structures). We will next describe some of these structures.

2.2.1 Sandwich

A sandwich structure is the general name for multilayered structures. They usually consist of two magnetic layers of an Fe–Co–Ni alloy, such as permalloy, separated by a non-magnetic conductive layer, such as Cu (Ranchal et al. 2002). A general scheme is shown in Figure 2.1a. With magnetic films of about 4–6 nm wide and a conductor layer of about 35 nm, magnetic coupling between layers is slightly small. With these configurations, MR levels of about 4%–9% are achieved, with linear ranges of about 50 Oe. The figures of merit of sandwich devices can be improved by continuously repeating the basic structure, thereby creating a multilayered system. Successful applications of sandwich structures in magnetic field sensing include bio-electronics (Mujika et al. 2009) and angle sensors (Lopez-Martin and Carlosena 2009).

2.2.2 Spin Valves

The origin of spin valves (SVs) comes from the sandwich structure. In SVs, an additional antiferromagnetic (pinning) layer is added to the top or bottom part of the structure, as shown in Figure 2.1b. In this sort of structure, there is

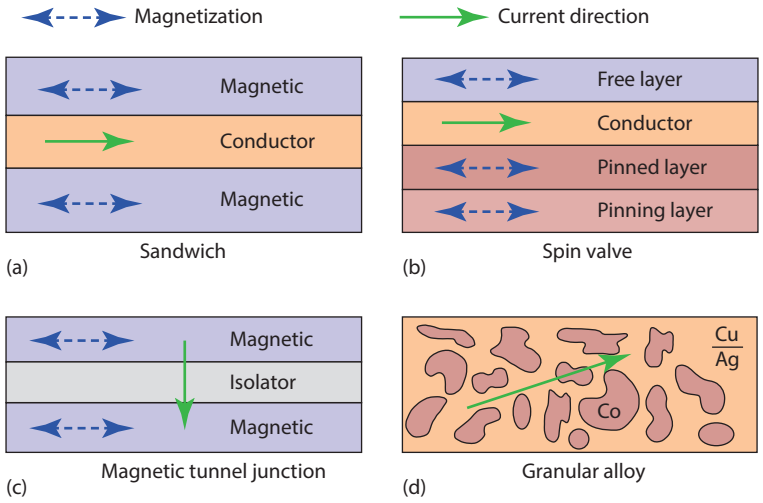

FIGURE 2.1
Basic structures displaying GMR phenomena.

no need for an external excitation to get the anti-parallel alignment. Despite this, the pinned direction (easy axis) is usually fixed by raising the temperature above the knee temperature (at which the antiferromagnetic coupling disappears) and then cooling it within a fixing magnetic field. Obviously, devices so obtained have a temperature limitation below the knee temperature. Typical values displayed by SVs are an MR of 4%–20% with saturation fields of 0.8–6 kA/m (Freitas et al. 2007).

For linear applications, and without excitation, pinned (easy axis) and free layers are arranged in a crossed-axis configuration (at 90°), as detailed in Figure 2.2a. The response of this structure is given by (Freitas et al. 2007)

$$\Delta R = \frac{1}{2}\left(\frac{\Delta R}{R}\right) R_{sq} i \frac{W}{h} \cos\left(\theta_p - \theta_f\right)$$

where:

$(\Delta R/R)$	is the maximum MR level (5%–20%)
R_{sq}	is the sensor sheet resistance (15–20 Ω/sq)
L	is the length of the element
W	is its width
h	is the thickness
i	is the sensor current
θ_p and θ_f	are the angle of the magnetization angle of the pinned and free layers, respectively

Assuming uniform magnetization for the free and pinned layers, for a linearized output, θ_p=90° and θ_f=0.

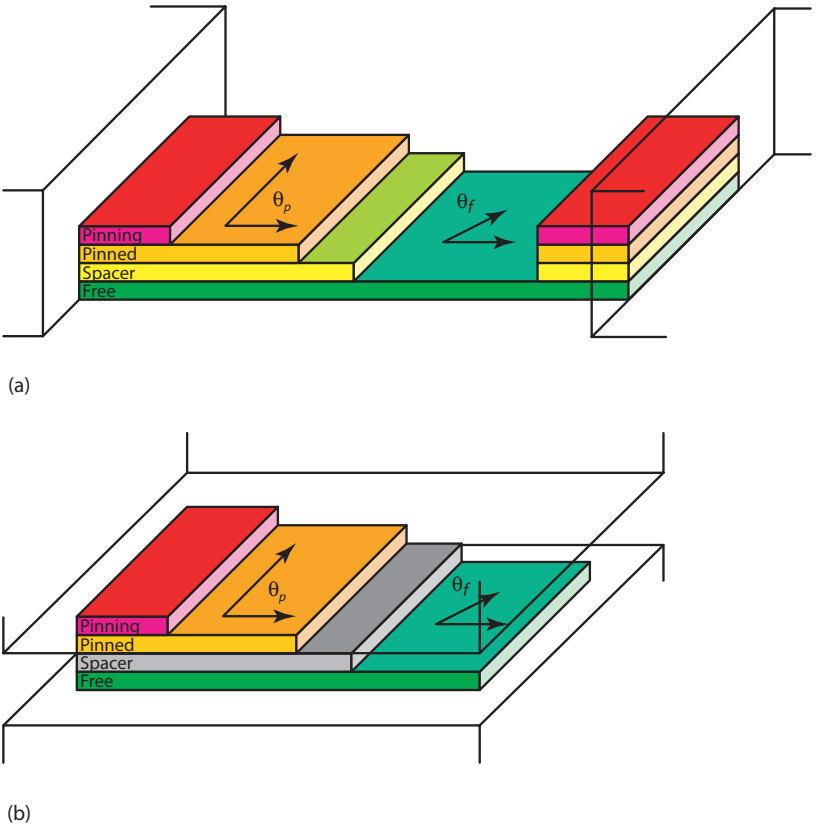

FIGURE 2.2
Multilayer structures corresponding to typical spin valves (a) and magnetic tunnel junctions (b).

2.2.3 Magnetic Tunnel Junctions

Magnetic tunnel junctions (MTJ), also called tunnel magnetoresistance (TMR) structures, were initially described as GMR structures (Hirota et al. 2002). Nowadays, they are considered a specific MR effect (Reig et al. 2013). Nevertheless, due to the similarity of both families of structures and their shared applications, we will also consider them in this chapter.

In this case, the magnetic layers are separated not by a conductive layer but by a very thin isolating layer, following a current perpendicular to planes (CPP) configuration (see Figures 2.1c and 2.2b). Electrons can cross this thin film by means of the quantum tunnel effect. As deduced from quantum mechanics arguments, the crossing probability is higher when both magnetic moments are aligned in parallel and lower when both magnetic moments are not aligned in parallel. The equation describing the output of these structures is

$$\Delta V = \frac{1}{2} \mathrm{TMR}\, i \frac{R \times A}{Wh} \cos\left(\theta_p - \theta_f\right)$$

where:

TMR	is the maximum MR level
i	is the biasing current
$R \times A$	is the resistance per area parameter
Wh	are the dimensions

These devices usually make use of the SV principle in order to fix the easy axis by means of a pinning antiferromagnetic layer. Typical MR levels of MTJ are above 40%, with Al_2O_3 as the isolating layer (Ziese and Thornton 2001). More recently, MR levels of about 200% have been reported for MgO-based structures (Ferreira et al. 2006). Saturation fields are of the order of 1–100 Oe. The basis of linear MTJs is analogous to that of a linear SV. When configured in a crossed-axis configuration, linear ranges suitable for sensor applications can be achieved (Freitas et al. 2007).

2.2.4 Other GMR Structures

Granular films of Co–Cu and Co–Ag also exhibit a GMR effect. In this case, the GMR effect is due to the spin-dependent scattering taking place at the boundaries of Co clusters embedded in the host lattice, as depicted in Figure 2.1d. Because these binary systems are not miscible, the characteristics of the devices are highly conditioned by the growth conditions and the post-deposition treatments. In fact, the amount of MR is accepted to be associated with the size of the Co clusters (Andrés et al. 1999).

GMR can also be found in other structures. We collected two illustrative examples. Pena et al. (2005) report on GMR in ferromagnet/superconductor superlattices and Pullini et al. (2007) describe GMR in multilayered nanowires. In any case, a magnetic–non-magnetic interface is required in order to allow the spin-electron scattering to produce the effect.

2.3 Devices

In order to have functional devices, GMR/TMR multilayered structures have to be patterned into elements with proper resistance values for use as sensors. Then, these elements need to be contacted.

2.3.1 Technological Issues

The deposition of these structures can be done with low temperature processes and then patterned by selective physical etching, so avoiding damage

in the substrate. In this sense, the deposition of these structures can be accomplished by ion beam deposition (IBD) or by sputtering. In any case, the substrate temperature does not exceed 120°C. Thus, both processes can be directly masked with photoresist without damaging the substrate. In some cases, a final heat treatment of between 200°C and 300°C is required to increase the MR ratio (He et al. 2010).

2.3.1.1 Spin Valves

A typical structure can be found in Reig et al. (2004). It was deposited by ion beam sputtering (IBD) onto a 3″ Si/SiO_2 1500 Å substrate. The SV structure was Ta (20 Å)/NiFe (30 Å)/CoFe (20 Å)/Cu (22 Å)/CoFe (25 Å)/MnIr (60 Å)/Ta (40 Å). This structure was demonstrated to give MR responses of about 6%–7%, linear ranges of about 20 Oe, and sheet resistivities of about 10–15 Ω/sq. Deposition rates ranged from 0.3 to 0.6 Å/s. A 40 Oe field was applied to the substrates during the deposition step in order to state the easy axis in the pinned and free layers. The wafer was rotated 90° between both depositions to ensure a crossed-axis SV configuration.

Nano-oxide layers (NOL) inserted in the pinned layer and above the free layer have been found to increase the MR ratio (Reig et al. 2005). The enhancement of GMR is attributed to the specular scattering effect of the conduction electrons at the metal–insulator interfaces.

2.3.1.2 Magnetic Tunnel Junctions

A typical MTJ structure was deposited by ion beam sputtering (IBD) onto 3″ Si/SiO_2 1000 Å substrates. The final structure of the MTJ was Al (600 Å)/Ta (90 Å)/NiFe (70 Å)/MnIr (250 Å)/CoFe (50 Å)/Al_2O_3 (12 Å)/CoFe (50 Å)/NiFe (25 Å)/Ta (60 Å)/TiW (300 Å), as described in Reig et al. (2008). This particular structure was demonstrated to give MR responses close to 40% while keeping linear ranges above 20 Oe.

2.3.2 Devices Design

To implement an SV-based device, only one lithographic step is required for patterning the structures (L1), and then another to design the contacts (L2), at the ends of the SV strip, as shown in Figure 2.3 (left). The sheet resistance is inherent to the specific SV structure, but the final resistance value can be tuned by properly setting L and W of the strip. Usually, the minimum W value is constrained by the lithography resolution, and then the L value is obtained. For SV structures such as those described in the Section 2.3.1.1, devices of 200×3 μm give nominal resistances of the order of 1 kΩ.

For MTJs, due to their CPP nature, two masks are required for defining an elemental device. In the first step, a mesa structure is defined (L1) (Figure 2.3, right). Then, a second mask (L2) is applied to define the pillars comprising

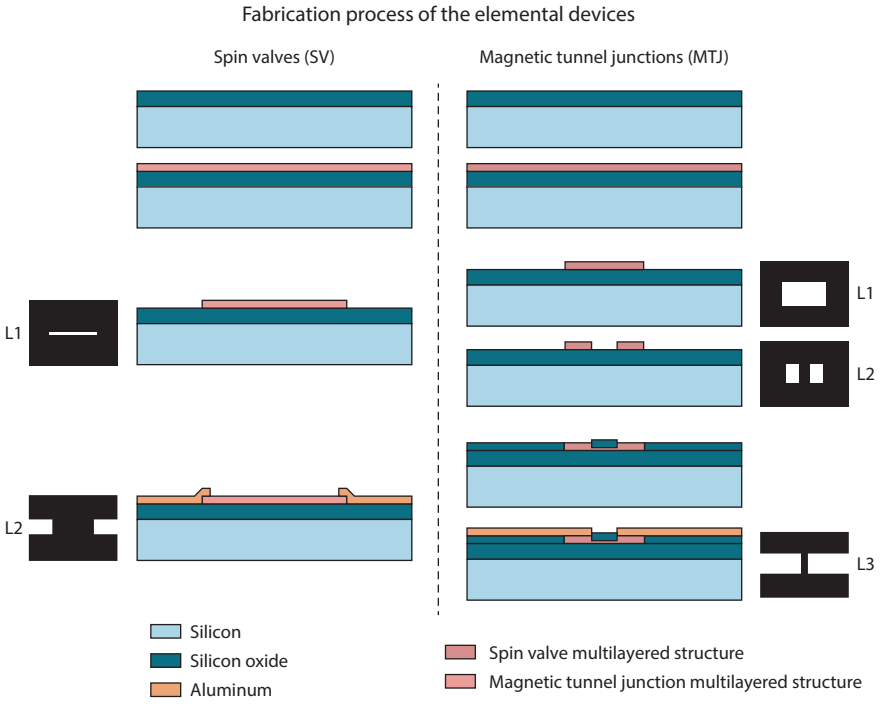

FIGURE 2.3
GMR/TMR basic fabrication steps.

the active region. Usually, a conductive bottom layer is included in the multilayered structure to connect devices in pairs, and facilitating the electrical contacts on the top of the structures (L3).

Because these elements are resistance, once they have been defined, they can be arranged in different configurations, depending on the specific requirement. MTJs are commonly arranged in arrays of elements in series and parallel, due to their better SNR performance and the intrinsic dependence of the MR level with the voltage bias (Chen and Freitas 2012).

In linear applications involving resistive sensors, bridge setups are often considered. They display a highly linear response, a better signal level, zeroed output, and high immunity to undesired external effects. Successful examples of the use of GMR/TMR sensors configured as bridges can be found in Cubells-Beltrán et al. (2009), Guerrero et al. (2009), and Le Phan et al. (2005).

When magnetic imaging is the objective, GMR sensors can also be arranged in arrays, as described, for example, by Cardoso et al. (2006), where MTJ elements have been integrated with a thin-film transistor (TFT) diode for improving the addressing process, or in Hall et al. (2013), where 256 pixels arrays with integrated complementary metal-oxide semiconductor (CMOS) circuitry have been demonstrated.

2.4 Limitations

The limitations of use of these sensors arise from very different reasons including the range of application, reproducibility, voltage offset, temperature drifts, or bandwidth constrictions. In the following sections, we describe some of these limitations and we give the direction of current investigations for overcoming them.

2.4.1 Range of Application

The intrinsically useful range of MR-based sensors is mainly limited by two mechanisms. At the low-level region, the SNR ratio sets the detection limit. Then, a study of the related noise sources is mandatory. The noise power spectrum density (PSD) is commonly given in square volts per hertz (V^2/Hz). Often, it is much more convenient to use the amplitude spectrum density (ASD), expressed in volts per square root hertz ($V/\sqrt{Hz}$), for a comparison with voltage signals. The sensitivity for an MR signal, S_V, is usually given in V/V/T. Typical values for GMR sensors are 20–40 V/V/T, for example, 20–40 nV/nT when they are biased with 1 V. For comparing different sensors, it is recommended to use the field equivalent noise power spectra density, sometimes called *detectivity*. It corresponds to the PSD divided by the sensitivity. For example, if a sensor displays a noise of 10 $nV/\sqrt{Hz}$ at a given frequency and a sensitivity of 25 V/V/T, its detectivity will be 400 pT for 1 V bias (Reig et al. 2013). At the high signal region, the saturation field is the limitation mechanism. For sensing applications, a good approximation is to consider the linear range to be one-half of the saturation field.

GMR/TMR can be applied in the range from some petatesles (pT) to almost kilotesles (kT), which is more than 14 orders of magnitude, as observed in Figure 2.4, compared with other magnetic sensors.

2.4.1.1 Noise Mechanisms in GMR/TMR Sensors

2.4.1.1.1 Thermal Noise

The most relevant noise is the thermal noise (also called the Johnson–Nyquist noise or white noise), which is directly related to the resistance of the sensor. It is a white noise, so it is independent of the frequency. It was first observed by Johnson (1928) and interpreted by Nyquist (1928). It is expressed as

$$S_V(\omega) = \sqrt{4Rk_BT}$$

where:

- R is the sensor resistance
- k_B is the Boltzmann constant
- T is the temperature

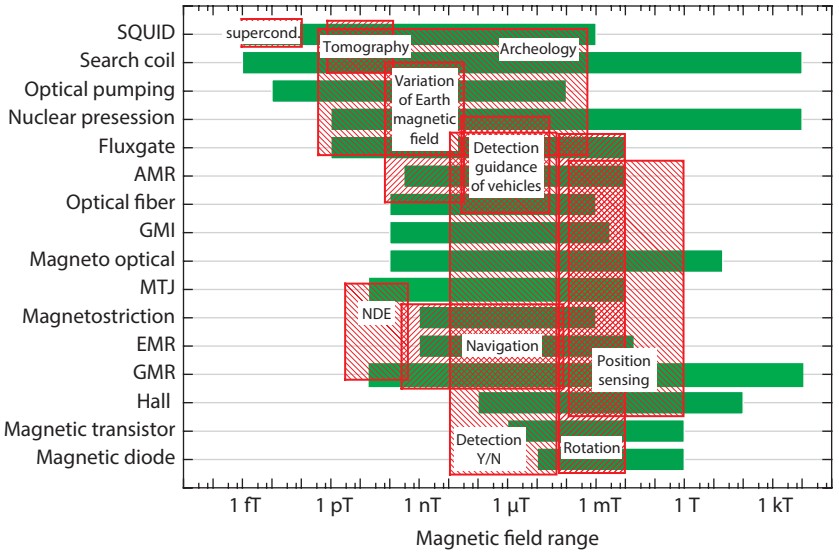

FIGURE 2.4
Range of applications of different magnetic field sensors. (From Díaz-Michelena, M., *Sensors* [*Basel, Switzerland*], 9(4), 2271–88, 2009.)

For example, a 1 kΩ resistor at room temperature has 4 nV/$\sqrt{\text{Hz}}$.

2.4.1.1.2 1/f Noise

The origin of the 1/*f* noise or "pink" noise or Flicker noise is from resistance fluctuations, so it can only be revealed by applying a current to the sensor. Its dependence with the frequency is described by the following phenomenological formula:

$$S_V(\omega) = \frac{\gamma_H R^2 I^2}{N_c f^{\beta}}$$

where:

- γ_H is a dimensionless constant proposed by Hooge (1976)
- R is the sensor resistance
- I is the bias current
- N_c is the number of current carriers
- f is the frequency
- β is an exponent typically of the order of 1

1/*f* noise can exhibit a non-magnetic and a magnetic component with possible different slopes. For TMRs, the formula becomes

$$S_V(\omega) = \frac{\alpha R^2 I^2}{A f}$$

where:

A is the active surface of the device

α is a parameter with the dimension of a surface

The size and shape of the sensors have a strong effect on the $1/f$ noise.

In GMRs and TMRs, this low-frequency noise is dominant and is often a drawback in the performance of the sensors. Although the TMR in MTJs is significantly higher than the MR in SVs, the intrinsic noise of an MTJ sensor is also higher than that of an SV (by a factor of about 3 [Freitas et al. 2007]). Due to its average nature, small GMR sensors display more $1/f$ noise than bigger sensors. By considering equally thin sensors, the $1/f$ noise is roughly inversely proportional to their area (Reig et al. 2013). As a graphical summary, Figure 2.5 shows the measured noise for several GMR commercial sensors, expressed as detectivity (Stutzke et al. 2005).

2.4.1.1.3 Random Telegraph Noise

The random telegraph noise (RTN; or "popcorn" noise) is due to the fluctuations of a specific source between two different levels with comparable energies and a barrier height able to give a typical characteristic time in the measurement range. RTN is difficult to handle and a sensor with RTN noise is in general very difficult to use even if it is theoretically possible to partially suppress this noise by data treatment.

2.4.1.1.4 Shot Noise

Shot noise (Freitas et al. 2007) arises in discontinuities in the conduction medium as a consequence of the discrete nature of the electrical charge and

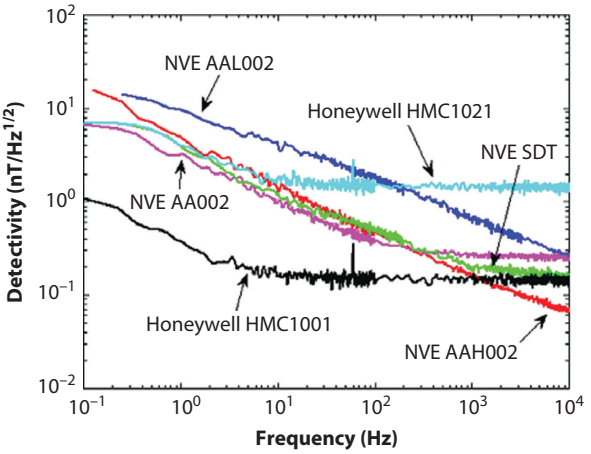

FIGURE 2.5
Low-frequency noise of commercial GMR sensors. (Reprinted with permission from Stutzke, N. A. et al., *Journal of Applied Physics* 97(10), 10Q107, 2005.)

is described by the following equation, where e stands for the electron electrical charge and I is the current flowing through the device (for practical device operating temperatures).

$$S_V(\omega) = 2eIR^2$$

The tunnel barrier of an MTJ is an example of a discontinuity in the conduction medium, which is why shot noise is found in MTJs but not in SVs or anisotropic magnetoresistance (AMR) sensors, which are made of continuous metallic layers.

2.4.2 Hysteresis

The magnetic nature of GMR-based sensors implies an associated hysteresis. Such effect has been analyzed for GMR sensors both numerically (Áč 2008) and experimentally (Liu et al. 2012). Intrinsically, this inherent hysteresis can be internally reduced by considering a so-called crossed-axis configuration of the magnetization moments of the constituent layers of the MR structure. In this case, since the free layer would never reverse, but merely displace by 90°, hysteretic errors below 1% of the full scale can be achieved (Reig et al. 2004). Alternating current (ac) biasing schemes have been proposed for reducing the hysteresis. In Ripka et al. (1999), by using an ac biasing of 5 mA at 10 kHz, the hysteresis of a commercial NVE sensor was reduced from 5% to 1% in the 0.3 mT range. In addition, both SNR and offset were also partially reduced. Hysteresis has also been reduced by biasing the sensors with an external magnetic field (Vopálenský et al. 2004). More recently, electrical models have been developed to reduce the hysteresis in specific GMR-based current sensors (Jedlicska et al. 2010; Han et al. 2015).

2.4.3 Voltage Offset

MR sensors are commonly used in a bridge configuration, so voltage offsets are introduced during the fabrication process. Common sources of these deviations are deposition inhomogeneities and lithography tolerances. As the dimensions of MR structures are close to the lithography resolution limit, these tolerances need to be externally corrected using external circuits.

2.4.4 Temperature Drifts

Temperature is always a limiting parameter in electronics. Every electronic device has a temperature-dependent response arising from its physical nature. Regarding specific GMR sensors, not only does the resistance (and the sensor impedance) vary with the temperature, but so does the MR level (and then the sensitivity).

The resistance of GMR sensors is a function of the temperature. For GMR-based devices, and in the usual range of utilization, this dependence can be considered linear, and can be defined by a temperature coefficient (TEMPCO) as follows:

$$\mathrm{TCR}(\%) = 100 \times \frac{1}{R_{T_0}} \frac{\Delta R}{\Delta T}$$

An analog relationship can be defined for the thermal dependence of sensitivity as

$$\mathrm{TCS}(\%) = 100 \times \frac{1}{S_{T_0}} \frac{\Delta \mathrm{S}}{\Delta T}$$

When a full bridge configuration is considered, this thermal dependence is partially compensated and is expected to be low. Due to the inherent voltage offset of sensors configured as bridges, the temperature drift of the offset voltage must be specified:

$$\mathrm{TCV}_{\mathrm{off}}(\%) = 100 \times \frac{\dfrac{\Delta V_{\mathrm{off}}}{\Delta T}}{V_{\mathrm{off},T_0}}$$

MR structures are temperature dependent. For real applications, the temperature coefficient of the output voltage of a given sensor can be set below 0.1%/K in a Wheatstone bridge configuration with a direct current (dc) bias instead of a direct voltage bias (Cubells-Beltrán et al. 2011). Experimental parameters are only related to the nature of the GMR structures, and they have been measured elsewhere. In Figure 2.6, we show the typical values for full bridge sensors composed of equal SV elements, as

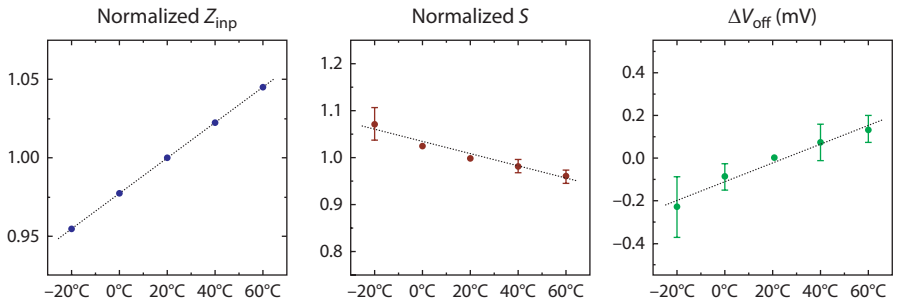

FIGURE 2.6
Temperature dependence of the characteristic parameters in typical spin valves. (From Cubells-Beltrán, M. et al., *IEEE Sensors Journal*, 9(12), 1756–62, 2009.)

described in Cubells-Beltrán et al. (2009). From these graphs, we can extract TCR ≈ 0.11%/°C, TCV_{off} < 10 μV/°C, and TCS ≈ −0.15%/°C, as they were defined before.

When thermal drifts are not sufficiently lowered by using bridge configurations, different temperature compensation schemes have been proposed in the literature, specifically developed for GMR sensors–based applications (Ramírez Muñoz et al. 2006; Sánchez Moreno et al. 2011).

2.4.5 Bandwidth

Theoretically, due to the inherent quantum mechanism involved, MR structures have bandwidths of the order of 1 GHz (Hirota et al. 2002). In real applications, a reduction in the bandwidth is introduced by the associated circuitry. Such an effect can be important in electric current monitoring applications because of the necessity to drive the current path close to the sensor. In principle, due to the inductive character of the coupling, a "zero" behavior in the transfer function should be observed. In Figure 2.7, the frequency responses of some illustrative examples are compiled: an HMC1O21 sensor soldered onto a typical (3 mm width) printed circuit board (PCB) strap, a meandered engineered SV sensor (Reig et al. 2004), and an MTJ compact current sensor prototype both in a full Wheatstone bridge configuration and a single resistor (Reig et al. 2008). As observed, an inductive effect appears well below 1 MHz. Moreover, the more complicated the sensing structure is, the less bandwidth obtained. Regarding real applications, MR current sensors have been successfully applied up to 1 MHz (Cubells-Beltrán et al. 2009; Singh and Khambadkone 2014).

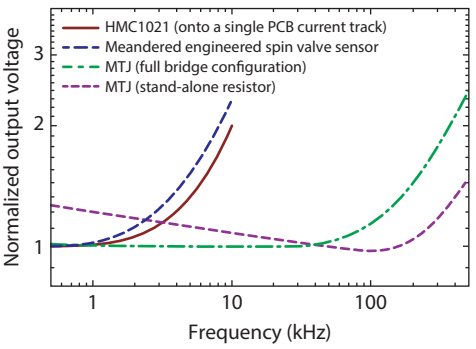

FIGURE 2.7
Frequency dependence of some selected GMR/MTJ current sensors. (From Cubells-Beltrán, M.-D. et al., *International Review of Electrical Engineering (IREE)* 6(1), 423–29, 2011.)

2.5 Applications

Now that we have described the principal characteristics of GMR/TMR sensors, we will describe some real applications in which these sensors have demonstrated their intrinsic capabilities.

2.5.1 General Purpose Magnetometers (Compass)

The measurement of the Earth's magnetic field is the ancient application of magnetic field sensors. The Earth's magnetic field ranges between approximately 25 and 60 μT, which is well covered by GMR/TMR sensors. With the increasing demand for digital compasses for mobile applications (mainly smartphones), GMR/TMR sensors have entered the market in serious competition with standard Hall solutions. Table 2.1 shows the main parameters of some selected MR compasses, including electronics (Reig et al. 2013).

2.5.2 Industrial Applications

2.5.2.1 Automotive

GMR sensors have entered the automotive market in several applications: steering angle measurement, rotor position measurement, speed sensing or crank shaft speed, and positions sensing. All of these can be classified as speed measurement or angle measurement. SV structures are commonly preferred for both sets of applications. A typical GMR angle sensor consists of several GMR resistors arranged in two bridges, one for each orthogonal direction (see Figure 2.8, left). Meandered geometries are used for increasing the total resistance to the kiloohms (kΩ) range. In this way, they provide a sine and a cosine signal that can be used in the calculation of the absolute angle of the magnetic field vector (see Figure 2.8, right). Due to this measurement principle, only the field direction, not the field magnitude, is relevant. The use of the GMR principle allows the measurement of angles in the full range of 360° in contrast to AMR-based sensors that cover only 180°. In any case, calibration of the devices is commonly required.

2.5.2.2 Space

In space sector applications, mass, volume, and power savings are important issues. GMR sensors are excellent candidates not only in planetary magnetometry, but also as magnetic encoders and angular or position sensors. It must be mentioned that space is an environment of extreme parameters, including wide temperature swings, very low pressures, moderate to high radiation, mechanical vibrations and impacts, and so on. GMR sensors have been used on several occasions in different satellite missions. As a summary, the evolution of MR

TABLE 2.1

Detailed Parameters of Selected Commercial Magnetoresistance-Based Compasses

General	Technology	AMR		GMR	MTJ
	Company	MEMSIC	Honeywell	Yamaha	Freescale
	Product	MMC314XMR	HMC5883L	YAS529	Mag3110
PKG	PKG	LGA10	LGA16	WLCSP10	DFN10
	Size (mm^3)	3 × 3 × 1	3 × 3 × 0.9	2 × 2 × 1	2 × 2 × 0.85
I/O	Voltage (V)	1.7–3.6	2.7–5.25	2.16–3.6	1.95–3.6
	Working current (mA)	~2	~2	4	>1
	Samples per s @mA	50 @ 0.55	7.5 @ 0.10	4	10 @ 0.14
	Interface	I2C	I2C	I2C	I2C
	Interrupt	–	–	–	Y
Maximum ratings	Storage temp (°C)	−55/+125	−40/+125	−50/+125	−40/+125
	Operating temp (°C)	−40/+85	−30/+85	−40/+95	−40/+85
	Max exposed field (G)	–	10k	2k	1k
Performance	Range (+/− G)	4	1–8	3	10
	ADC (output bits)	12	12	10	15
	Resolution (mG)	2	2	6 (x,y)/12 (z)	1
	Offset (+/− G)	0.2	–	–	0.01
	Accuracy (°)	2	2	5	–
	Linearity (%FS)	1	0.1	–	1
	Hysteresis (%FS)	0.1	0.0025	–	1
	Repeatability (%FS)	–	0.1	–	–
	Sensitivity TC (%/°)	0.11	–	–	0.1
	Offset TC (mG/°)	0.4	–	–	0.1
	Bandwidth (Hz)	40	75	40	40
	Noise (RMS)	0.6 mG @ 25 Hz	–	–	0.5 mG
Features	On-chip temp sensor	Y	–	Y	Y
	Single-chip integration	–	–	Y	–
	Offset removal	Y	Y	–	–
	Self test	–	Y	–	–
	Others			3 external AD	Oversampling

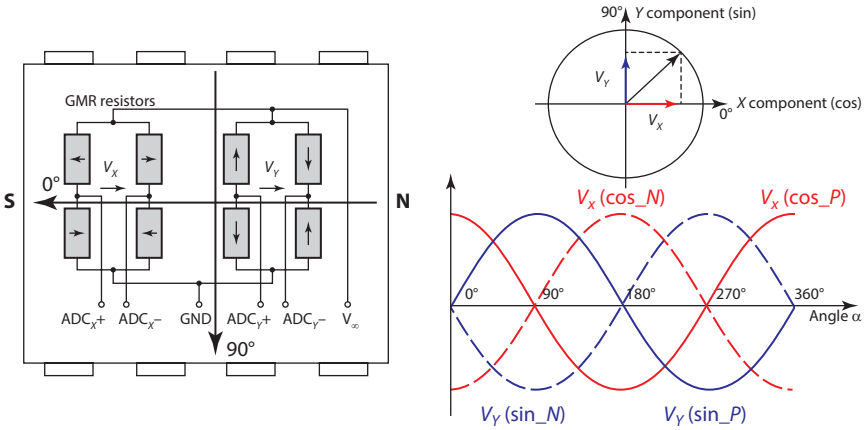

FIGURE 2.8
Typical arrangement of GMR angle sensors for automotive applications.

technologies in space applications is depicted in Figure 2.9 (Díaz-Michelena 2009).

2.5.2.3 Electric Current Measurement

Traditional methods for measuring an electric current include shunt resistors and the transformer principle, and its indirect measurement is by means of the generated magnetic field (Ziegler et al. 2009). This latter scheme has successfully approached making use of different magnetic field sensors (Pavel Ripka and Janosek 2010). In this sense, GMR sensors display some intrinsic properties, making them optimal for electric current measurement schemes, namely, high sensitivity, capable of integrating with other technologies (PCB or CMOS), and the measurement of in-plane magnetic fields. An extensive review on the application of GMR sensors in electrical current measurement can be found in Reig et al. (2009). The basic scheme is very simple: we just need to drive the desired current path to the neighborhood of the sensor, as depicted in Figure 2.10a. The sensor can be placed either above or below the current path. As observed, the magnetic field lines fall almost parallel to the sensor layers.

Sensing performance can be improved by using a bridge configuration. When the current path is already defined (usually a straight line), a scheme, as shown in Figure 2.10b1, with a half bridge is applicable. In this case, R_1 and R_3 are active and R_2 and R_4 are usually shielded as suggested, for example, in Singh and Khambadkone (2008) or Vieth et al. (2000). To get the full bridge behavior, we can fabricate the sensor with four active (opposite) elements (Pelegri Sebastia et al. 2004) or actuate on the design of the current path, as illustrated in Figure 2.10b2–b4. The successful application of these schemes can be found in Sanchez et al. (2012) and Pannetier-Lecoeur

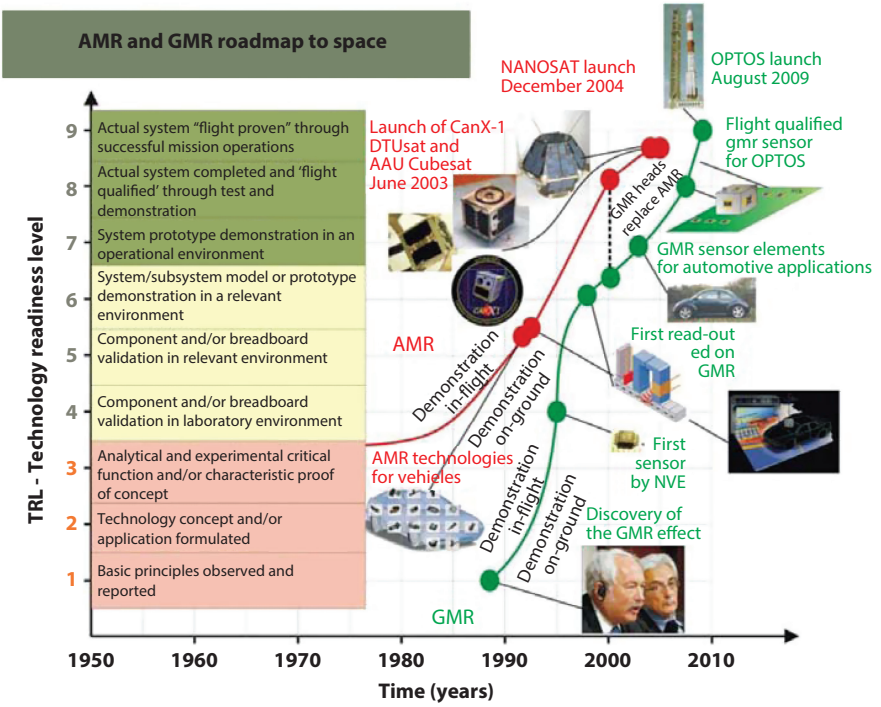

FIGURE 2.9
Recent history of AMR and GMR technologies in space applications. (From Díaz-Michelena, M., *Sensors (Basel, Switzerland)*, 9(4), 2271–88, 2009.)

et al. (2007) (Figure 2.10b2); Reig et al. (2004) and Cubells-Beltrán et al. (2009) (Figure 2.10b3); and Reig et al. 2005 and Cubells-Beltrán et al. (2009) (Figure 2.10b4). For an optimal geometric design of the current paths and the position of the sensors, numerical models (mainly the finite element method [FEM]) are commonly used (Beltran et al. 2007).

Limitations on the performance of GMR-based current sensors arise mainly from packaging issues (Cubells-Beltrán et al. 2011). Most significant is heating from the joule effect because of current and bandwidth constraints due to the capacitive/inductive coupling of the current path. Thermal drifts due to joule heating (Vopalensky and Platil 2013) can be significant not only in medium/high current applications, but also in integrated circuits (ICs) environments. They can be reduced either with the use of full Wheatstone bridge sensors (Reig et al. 2004; Cubells-Beltrán et al. 2009) or with the use of external compensation electronic circuitry (Ramírez Muñoz et al. 2006; Sánchez Moreno et al. 2011). To properly analyze such effects, numerical modeling is commonly used, from both a physical (Beltran et al. 2007) and an electrical point of view (Roldán et al. 2010a).

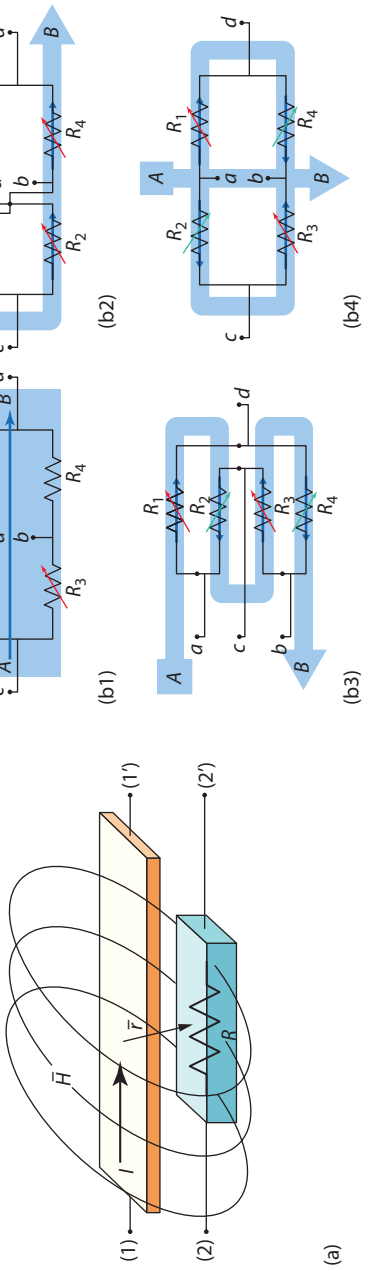

FIGURE 2.10
Current measurement with GMR sensors: (a) principle description, (b) different geometrical approaches.

Specific applications of GMR sensors for electrical current measurement include built-in current sensing (BICS) schemes in ICs. This was first demonstrated in 2005 (Reig et al. 2005) and then improved with low noise devices (Pannetier-Lecoeur et al. 2007), using MTJ sensors (Le Phan et al. 2005), full bridge arrangements (Cubells-Beltrán et al. 2009), and improved conditioning circuitry (Madrenas et al. 2014). Electric currents in the range of 1 μA have been resolved in this way. In addition, these schemes have become successful when integrated with standard CMOS technologies (Cubells-Beltrán et al. 2014).

We should also mention that GMR sensors have also been used in related applications such as analog electric isolators (Reig et al. 2008) and integrated wattmeters (Roldán et al. 2010b).

2.5.3 Non-Destructive Evaluation

Non-destructive evaluation (NDE) refers to any examination, test, or evaluation performed on any type of object without changing or altering it in any way, in order to determine the absence (or presence) of discontinuities that could jeopardize its functionality. The most common NDE methods are optical inspection (including non-visible range such as infrared or x-rays), ultrasonic tests, and magnetic measurements.

2.5.3.1 Magnetic Detection

As mentioned, magnetic measurements are commonly used in NDE in general and scan systems (imaging or detecting) in particular. We can measure the magnetic field of the scanned objects (if existing) or the perturbation that they produce in the Earth's magnetic field. Traditionally, pick-up coils and Hall sensors have been used. We will enumerate some of the successful applications in which GMR sensors have been considered in these scenarios.

GMR sensors have been successfully used for the detection/monitoring of different kinds of objects, including traffic speed monitoring (Pelegrí Sebastiá et al. 2007), tool vibration (Sebastia et al. 2009), weapon detection (Tian et al. 2012), localization of hidden metallic objects (Renhart et al. 2011), robot movement control (Ku et al. 2000), and even electric guitar monitoring (Lenssen et al. 2002).

Regarding specific imaging techniques (also scanning microscopy), GMR sensors have been applied to the evaluation of current faults at the IC level with sub-micron resolution involving electric currents below 1 mA (Reig et al. 2013). The magnetic field microscopy of rock samples using a GMR-based scanning magnetometer has also been reported (Hankard et al. 2009).

2.5.3.2 Eddy Current Testing

Within magnetic field–based techniques, eddy current testing (ECT) has been specifically considered in a wide range of modern testing processes, including defects in metallic surfaces and subsurfaces.

Eddy currents are closed loops of induced current circulating in a plane that is perpendicular to the direction of a time-varying magnetic flux density $\boldsymbol{B}$, as depicted in Figure 2.11. The variation of $\boldsymbol{B}$ generates an electric field intensity $\boldsymbol{E}$, in a loop as expressed by the Maxwell equation:

$$\nabla \times \mathbf{E} = -\frac{\partial \mathbf{B}}{\partial t}$$

Therefore, the current density $\boldsymbol{J}$, in a material with conductivity σ, also circulates in the loop, because

$$\mathbf{J} = \sigma \mathbf{E}$$

Such currents, due to conductivity σ, can degrade the performance of the affected surfaces, but they can also be used for detecting flaws or cracks on metallic materials, conductivity variations, spacing between probe and device under test, material thickness, thickness of platting or cladding on a base material, spacing between conductive layers, or permeability variations.

The concept of using GMR in ECT measurements was first introduced by Dogaru and Smith (2001), through two geometrical approaches taking advantage of the inherent properties of GMR sensors, as detailed in Figure 2.11. In this particular experiment, currents of the order of 1 A at 30 kHz were used for the exciting coils, and NVE commercial unipolar devices (~25 mV/V/mT sensitivity, 2 mT, linear range) as GMR sensors. In this way, cracks 1–15 mm long, 0.5 mm wide, and 0.25–4 mm deep were

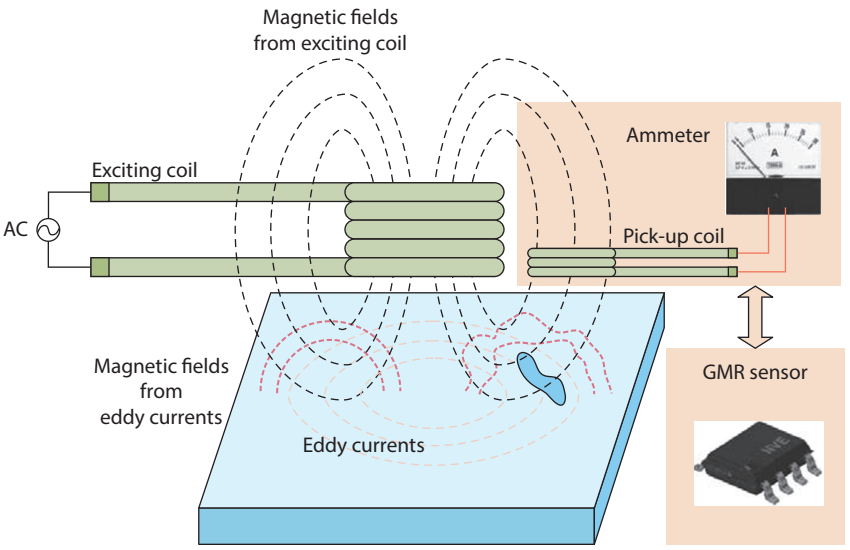

FIGURE 2.11
Scheme of an eddy current testing system, with a GMR as sensing element.

scanned. A similar system with portable characteristics is described in Betta et al. 2012). By including a feedback coil in the scheme in Figure 2.12, resolution in depth can be achieved (Jeng et al. 2006). The depth of the defects can also be detected (Espina-Hernández et al. 2012). In this scenario, the use of numerical models (mainly based on FEM) is highly helpful (Zeng et al. 2011).

ECT based on GMR sensors has been extensively applied to the evaluation of PCBs. Initially, Chomsuwan and co-workers (Yamada et al. 2004) demonstrated it with a specifically designed SV sensor (200 mV/mT sensitivity) with a printed meandered coil, by mapping PCB defects of the order of 100 μm size. These results were better than those obtained with a pick-up coil–based system. Novel experiments were performed on high-density double-layer PCBs with an improved ECT probe including an optimized meander coil and an array of GMR sensors (Chomsuwan et al. 2005, 2007a,b). Defects with sizes below 100 μm were resolved on both sides of the PCB. This topic is revisited frequently (Cacciola et al. 2011).

The ECT technique based on GMR sensors has also been applied to the evaluation of the health of an aircraft's structure (Nair et al. 2006). Pulsed currents have been demonstrated to improve the performance of ECT probes in this sense (Tamburrino et al., 2010).

2.5.4 Bio-Applications

Magnetic fields (generated and/or measured) are extensively used in biologic sciences including genetics, bio-technology, different fields of medicine (physiology, oncology, etc.), among others. Most of these applications require the measurement of very low magnetic fields (below the nT limit) in small spaces (commonly in the sub-mm range). At the beginning of the century, MR sensors started to be explored as the sensing elements in biochips. A biosensor can be defined as a "compact analytical device or unit incorporating a biological or biologically-derived sensitive element integrated or associated with a physio-chemical transducer" (Graham et al. 2004).

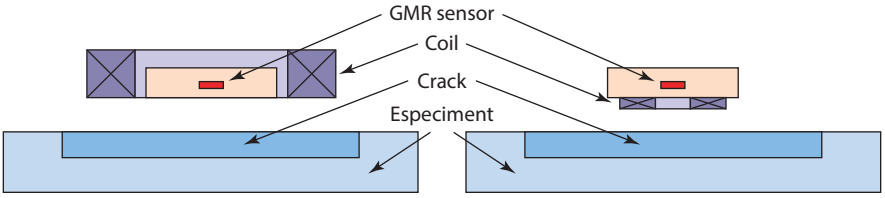

FIGURE 2.12
Different arrangements for integrating GMR sensors with exciting coils in ECT systems.

2.5.4.1 Detection of Bioanalytes

General bioanalytes (molecules, cells, viruses, bacteria, tissues) are not magnetic. In order to take advantage of GMR for monitoring or detecting bioanalytes, they must be bonded to magnetic elements (usually nanoparticles [NPs]) (Wang et al. 2014; Lee et al. 2009) and driven near the sensor by means of microfluidics (Muluneh and Issadore 2014) or guiding magnetic fields (Giouroudi and Keplinger 2013; Gooneratne et al. 2011). GMR sensors have been successfully applied to the detection of proteins (Gaster et al. 2011), DNA (Wang et al. 2013), viruses (Zhi et al. 2014), and bacteria (Mujika et al. 2009). In this way, two approaches can be defined: static and dynamic, as depicted in Figure 2.13.

An example of the static approach is the analysis of DNA (Koets et al. 2009). For DNA detection, single-stranded DNA receptors are first immobilized on the surface of magnetic sensors. Oligonucleotides of unknown sequence are selectively captured by complementary probes. SA-coated magnetic NPs are then introduced and bind to the biotin of the hybridized DNA. Finally, magnetic field disturbances because of the NPs are sensed by magnetic sensors. Biotin and streptavidin are often used in this process (Wang et al. 2013). To improve the performance of the sensor system, microcoils can be integrated in association with the sensing elements. These coils generate a magnetic field that is used to attract the magnetic beads to the sensor area and activate them (Freitas et al. 2011). In this way, the femtomolar limit of detection has been achieved.

For the detection of general cells (cytometry), magnetic nanobeads need to be bonded to them (Freitas et al. 2012). Then, by means of microfluidics or guiding magnetic fields, they are driven close to the sensors, where the detection is performed, as described in Shoshi et al. (2012).

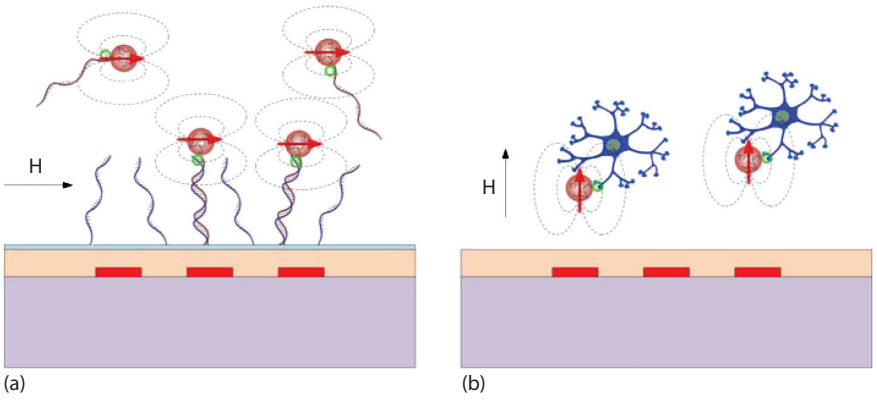

FIGURE 2.13
Static (a) and dynamic (b) approaches for bioanalytes detection with GMR sensors.

2.5.4.2 Monitoring of Magnetic Fluids

Fluids incorporating magnetic particles (usually nanobeads) are known as *magnetic fluids*. They can be made biocompatible for *in vivo* applications, such as hyperthermia cancer therapy. A magnetic fluid is injected into the affected area and an external ac magnetic flux density is applied to exploit the self-heating properties of the magnetic beads in the fluid. Temperatures in excess of 42°C destroy tumors (Reig et al. 2013). Hence, the accurate estimation of magnetic fluid content density is critical for the success of the treatment. In Mukhopadhyay et al. (2007), a GMR-based needle probe 20 mm long and 310 μm wide, comprising four SV sensors was analyzed. The needle probe was successfully tested in tumor-simulating cylindrical agar cavities.

2.5.4.3 Biomedical Signal Detection

GMR/TMR-based micromachined probe needles have also been designed for detecting brain activity through the measurement of generated magnetic fields. After demonstrating the concept (Amaral et al. 2011), MTJ-based microneedles were developed and characterized (Amaral et al. 2013). The associated electronics were also specifically implemented (Costa et al. 2014).

A non-invasive detection system for magnetocardiography applications has also been described by Pannetier-Lecoeur et al. (2010), where a GMR sensor is integrated with a high-temperature superconductor (YBCO).

2.6 Conclusions

GMR/TMR sensors have rapidly passed their initial potentiality in real applications and have become the first option in a huge number of scenarios demanding the measurement of low magnetic fields with a high level of integration devices. Complete knowledge of the underlying phenomena has allowed the specific design of different kinds of devices. Their SNR, and subsequent detectivity, make them suitable for most applications in different fields such as bio-technology, microelectronics, and space.

Acknowledgments

The authors are grateful for the very fruitful collaborations that have made possible some of the results presented in this chapter: INESC-MN (Lisboa, Portugal), University of L'Aquila (Italy), UPC (Barcelona, Spain), and CNM (Barcelona, Spain).

References

Ač, V. 2008. A study of hysteresis in the GMR layer structures by FEM. *Physica B: Condensed Matter* 403 (2–3): 460–63.

Amaral, J., S. Cardoso, P. P. Freitas, and A. M. Sebastião. 2011. Toward a system to measure action potential on mice brain slices with local magnetoresistive probes. *Journal of Applied Physics* 109 (7): 07B308.

Amaral, J., V. Pinto, T. Costa, J. Gaspar, R. Ferreira, E. Paz, S. Cardoso, and P. P. Freitas. 2013. Integration of TMR sensors in silicon microneedles for magnetic measurements of neurons. *IEEE Transactions on Magnetics* 49 (7): 3512–15.

Andrés, J. P., J. Colino, and J. M. Riveiro. 1999. Enhancement of GMR in as-deposited Co-Cu granular films with RF sputtering power. *Journal of Magnetism and Magnetic Materials* 196–197 (May): 493–94.

Baibich, M. N., J. M. Broto, A. Fert, F. N. Vandau, F. Petroff, P. Eitenne, G. Creuzet, A. Friederich, and J. Chazelas. 1988. Giant magnetoresistance of (001)Fe/(001)Cr magnetic superlattices. *Physical Review Letters* 61 (21): 2472–75.

Beltran, H., C. Reig, V. Fuster, D. Ramírez, and M. D. Cubells-Beltrán. 2007. Modeling of magnetoresistive-based electrical current sensors: A technological approach. *IEEE Sensors Journal* 7 (11): 1532–37.

Betta, G., L. Ferrigno, and M. Laracca. 2012. GMR-based ECT instrument for detection and characterization of crack on a planar specimen: A hand-held solution. *IEEE Transactions on Instrumentation and Measurement* 61 (2): 505–12.

Binasch, G., P. Grunberg, F. Saurenbach, and W. Zinn. 1989. Enhanced magnetoresistance in layered magnetic-structures with antiferromagnetic interlayer exchange. *Physical Review B* 39 (7): 4828–30.

Cacciola, M., G. Megali, D. Pellicanó, and F. C. Morabito. 2011. A GMR–ECT based embedded solution for applications on PCB inspections. *Sensors and Actuators A: Physical* 167 (1): 25–33.

Cardoso, F. A., H. A. Ferreira, J. P. Conde, V. Chu, P. P. Freitas, D. Vidal, J. Germano, et al. 2006. Diode/magnetic tunnel junction cell for fully scalable matrix-based biochip. *Journal of Applied Physics* 99 (8): 08B307.

Chen, X., and P. P. Freitas. 2012. Magnetic tunnel junction based on MgO barrier prepared by natural oxidation and direct sputtering deposition. *Nano-Micro Letters* 4 (1): 25–29.

Chomsuwan, K., S. Yamada, and M. Iwahara. 2007a. Improvement on defect detection performance of PCB inspection based on ECT technique with multi-SV-GMR sensor. *IEEE Transactions on Magnetics* 43 (6): 2394–96.

Chomsuwan, K., S. Yamada, and M. Iwahara. 2007b. Bare PCB inspection system with SV-GMR sensor eddy-current testing probe. *IEEE Sensors Journal* 7 (5): 890–96.

Chomsuwan, K., S. Yamada, M. Iwahara, H. Wakiwaka, and S. Shoji. 2005. Application of eddy-current testing technique for high-density double-layer printed circuit board inspection. *IEEE Transactions on Magnetics* 41 (10): 3619–21.

Costa, T., M. S. Piedade, J. Germano, J. Amaral, and P. P. Freitas. 2014. A neuronal signal detector for biologically generated magnetic fields. *IEEE Transactions on Instrumentation and Measurement* 63 (5): 1171–80.

Cubells-Beltrán, M. D., C. Reig, A. De Marcellis, E. Figueras, A. Yúfera, B. Zadov, E. Paperno, S. Cardoso, and P. P. Freitas. 2014. Monolithic integration of giant magnetoresistance (GMR) devices onto standard processed CMOS dies. *Microelectronics Journal* 45 (6): 702–7.

Cubells-Beltrán, M.-D., C. Reig, J. Martos, J. Torres, and J. Soret. 2011. Limitations of magnetoresistive current sensors in industrial electronics applications. *International Review of Electrical Engineering (IREE)* 6 (1): 423–29.

Cubells-Beltrán, M. D., C. Reig, D. R. Muñoz, S. I. P. C. de Freitas, and P. J. P. De Freitas. 2009. Full Wheatstone bridge spin-valve based sensors for IC currents monitoring. *IEEE Sensors Journal* 9 (12): 1756–62.

Díaz-Michelena, M. 2009. Small magnetic sensors for space applications. *Sensors (Basel, Switzerland)* 9 (4): 2271–88.

Dogaru, T., and S. T. Smith. 2001. Giant magnetoresistance-based eddy-current sensor. *IEEE Transactions on Magnetics* 37 (5): 3831–38.

Espina-Hernández, J. H., E. Ramírez-Pacheco, F. Caleyo, J. A. Pérez-Benitez, and J. M. Hallen. 2012. Rapid estimation of artificial near-side crack dimensions in aluminium using a GMR-based eddy current sensor. *NDT & E International* 51 (October): 94–100.

Ferreira, R., P. Wisniowski, P. P. Freitas, J. Langer, B. Ocker, and W. Maass. 2006. Tuning of MgO barrier magnetic tunnel junction bias current for picotesla magnetic field detection. *Journal of Applied Physics* 99 (8): 08K706.

Freitas, P. P., F. A. Cardoso, V. C. Martins, S. A. M. Martins, J. Loureiro, J. Amaral, R. C. Chaves, et al. 2012. Spintronic platforms for biomedical applications. *Lab on a Chip* 12 (3): 546–57.

Freitas, P. P., S. Cardoso, R. Ferreira, V. C. Martins, A. Guedes, F. A. Cardoso, J. Loureiro, R. Macedo, R. C. Chaves, and J. Amaral. 2011. Optimization and integration of magnetoresistive sensors. *SPIN* 01 (01): 71–91.

Freitas, P. P., R. Ferreira, S. Cardoso, and F. Cardoso. 2007. Magnetoresistive sensors. *Journal of Physics: Condensed Matter* 19 (16). IOP Publishing: 165221.

Gaster, R. S, L. Xu, S-J. Han, R. J. Wilson, D. A. Hall, S. J. Osterfeld, H. Yu, and S. X. Wang. 2011. Quantification of protein interactions and solution transport using high-density GMR sensor arrays. *Nature Nanotechnology* 6 (5): 314–20.

Giouroudi, I., and F. Keplinger. 2013. Microfluidic biosensing systems using magnetic nanoparticles. *International Journal of Molecular Sciences* 14 (9): 18535–56.

Gooneratne, C. P., C. Liang, and J. Kosel. 2011. A planar conducting microstructure to guide and confine magnetic beads to a sensing zone. *Microelectronic Engineering* 88 (8): 1757–60.

Graham, D. L., H. A. Ferreira, and P. P. Freitas. 2004. Magnetoresistive-based biosensors and biochips. *Trends in Biotechnology* 22 (9): 455–62.

Guerrero, R., M. Pannetier-Lecoeur, C. Fermon, S. Cardoso, R. Ferreira, and P. P. Freitas. 2009. Low frequency noise in arrays of magnetic tunnel junctions connected in series and parallel. *Journal of Applied Physics* 105 (11): 113922.

Hall, D. A., R. S. Gaster, K. Makinwa, S. X. Wang, and B. Murmann. 2013. A 256 pixel magnetoresistive biosensor microarray in 0.18μm CMOS. *IEEE Journal of Solid-State Circuits* 48 (5): 1290–1301.

Han, J., J. Hu, Y. Ouyang, S. X. Wang, and J. He. 2015. Hysteretic modeling of output characteristics of giant magnetoresistive current sensors. *IEEE Transactions on Industrial Electronics* 62 (1): 516–24.

Hankard, F., J. Gattacceca, C. Fermon, M. Pannetier-Lecoeur, B. Langlais, Y. Quesnel, P. Rochette, and S. A. McEnroe. 2009. Magnetic field microscopy of rock samples using a giant magnetoresistance-based scanning magnetometer. *Geochemistry, Geophysics, Geosystems* 10: Q10Y06.

He, H., K. Zhernenkov, M. Vadalá , N. Akdogan, D. Gorkov, R. M. Abrudan, B. P. Toperverg, H. Zabel, H. Kubota, and S. Yuasa. 2010. The effect of annealing on the junction profile of CoFeB/MgO tunnel junctions. *Journal of Applied Physics* 108 (6): 063922.

Hirota, E., H. Sakakima, and K. Inomata. 2002. *Giant Magneto-Resistance Devices*. Vol. 40. Springer Series in Surface Sciences. Berlin: Springer. doi:10.1007/978-3-662-04777-4.

Hooge, F. N. 1976. 1/*f* noise. *Physica B+C* 83 (1): 14–23.

Jedlicska, I., R. Weiss, and R. Weigel. 2010. Linearizing the output characteristic of GMR current sensors through hysteresis modeling. *IEEE Transactions on Industrial Electronics* 57 (5): 1728–34.

Jeng, J.-T., G-S. Lee, W-C. Liao, and C-L. Shu. 2006. Depth-resolved eddy-current detection with GMR magnetometer. *Journal of Magnetism and Magnetic Materials* 304 (1): e470–73.

Johnson, J. B. 1928. Thermal agitation of electricity in conductors. *Physical Review* 32 (1): 97–109.

Koets, M., T. van der Wijk, J. T. W. M. van Eemeren, A. van Amerongen, and M. W. J. Prins. 2009. Rapid DNA multi-analyte immunoassay on a magneto-resistance biosensor. *Biosensors and Bioelectronics* 24 (7): 1893–98.

Ku, W., P. P. Freitas, P. Compadrinho, and J. Barata. 2000. Precision X-Y robotic object handling using a dual GMR bridge sensor. *IEEE Transactions on Magnetics* 36 (5): 2782–84.

Le, P., K., H. Boeve, F. Vanhelmont, T. Ikkink, and W. Talen. 2005. Geometry optimization of TMR current sensors for on-chip IC testing. *IEEE Transactions on Magnetics* 41 (10): 3685–87.

Lee, K., S. Lee, B. K. Cho, K-S. Kim, and B. Kim. 2009. The limit of detection of giant magnetoresistive (GMR) sensors for bio-applications. *Journal of the Korean Physical Society* 55 (1): 193–96.

Lenssen, K.-M. H., G. H. J. Somers, and J. B. A. D. van Zon. 2002. Magnetoresistive sensors for string instruments. *Journal of Applied Physics* 91 (10): 7777.

Liu, S., Q. Huang, Y. Li, and W. Zhen. 2012. Experimental research on hysteresis effects in GMR sensors for analog measurement applications. *Sensors and Actuators A: Physical* 182 (August): 72–81.

Lopez-Martin, A. J., and A. Carlosena. 2009. Performance tradeoffs of three novel GMR contactless angle detectors. *IEEE Sensors Journal* 9 (3): 191–98.

Madrenas, J., M.-D. Cubells-Beltrán, B. Zadov, S. Cardoso, C. Reig, P. P. Freitas, E. Paperno, and A. De Marcellis. 2014. Quasi-digital front-ends for current measurement in integrated circuits with giant magnetoresistance technology. *IET Circuits, Devices {&} Systems* 8 (4): 291–300.

Mujika, M., S. Arana, E. Castaño, M. Tijero, R. Vilares, J. M. Ruano-López, A. Cruz, L. Sainz, and J. Berganza. 2009. Magnetoresistive immunosensor for the detection of *Escherichia coli* O157:H7 including a microfluidic network. *Biosensors & Bioelectronics* 24 (5): 1253–58.

Mukhopadhyay, S. C., K. Chomsuwan, C. P. Gooneratne, and S. Yamada. 2007. A novel needle-type SV-GMR sensor for biomedical applications. *IEEE Sensors Journal* 7 (3): 401–8.

Muluneh, M., and D. Issadore. 2014. A multi-scale PDMS fabrication strategy to bridge the size mismatch between integrated circuits and microfluidics. *Lab on a Chip* 14 (23): 4552–58.

Nair, N. V., V. R. Melapudi, H. R. Jimenez, X. Liu, Y. Deng, Z. Zeng, L. Udpa, T. J. Moran, and S. S. Udpa. 2006. A GMR-based eddy current system for NDE of aircraft structures. *IEEE Transactions on Magnetics* 42 (10): 3312–14.

Nyquist, H. 1928. Thermal agitation of electric charge in conductors. *Physical Review* 32 (1): 110–13.

Pannetier-Lecoeur, M., C. Fermon, A. de Vismes, E. Kerr, and L. Vieux-Rochaz. 2007. Low noise magnetoresistive sensors for current measurement and compasses. *Journal of Magnetism and Magnetic Materials* 316 (2): e246–48.

Pannetier-Lecoeur, M., C. Fermon, H. Dyvorne, J. F. Jacquinot, H. Polovy, and A. L. Walliang. 2010. Magnetoresistive-superconducting mixed sensors for biomagnetic applications. *Journal of Magnetism and Magnetic Materials* 322 (9–12): 1647–50.

Pelegrí Sebastiá, J., J. Alberola Lluch, and J. Rafael Lajara Vizcaíno. 2007. Signal conditioning for GMR magnetic sensors applied to traffic speed monitoring. *Sensors and Actuators A: Physical* 137 (2): 230–35.

Pelegri Sebastia, J., D. R. Munoz, and P. J. P. de Freitas. 2004. A novel spin-valve bridge sensor for current sensing. *IEEE Transactions on Instrumentation and Measurement* 53 (3): 877–80.

Peña, V., Z. Sefrioui, D. Arias, C. Leon, J. Santamaria, J. L. Martinez, S. G. E. Te Velthuis, and A. Hoffmann. 2005. Giant magnetoresistance in ferromagnet/superconductor superlattices. *Physical Review Letters* 94 (5): 057002.

Pullini, D., D. Busquets, A. Ruotolo, G. Innocenti, and V. Amigó. 2007. Insights into pulsed electrodeposition of GMR multilayered nanowires. *Journal of Magnetism and Magnetic Materials* 316 (2): e242–45.

Ramírez Muñoz, D., J. Sánchez Moreno, S. Casans Berga, E. Castro Montero, C. Reig Escrivà, and A. Edith Navarro Antón. 2006. Temperature compensation of Wheatstone bridge magnetoresistive sensors based on generalized impedance converter with input reference current. *Review of Scientific Instruments* 77 (10): 105102.

Ranchal, R., M. Torija, E. López, M. C. Sánchez, C. Aroca, and P. Sánchez. 2002. The influence of anisotropy on the magnetoresistance of permalloy-copper-permalloy thin films. *Nanotechnology* 13 (3): 392–97.

Reig, C., S. Cardoso, and S. Mukhopadhyay. 2013. *Giant Magnetoresistance (GMR) Sensors: From Basis to State-of-the-Art Applications*. Berlin: Springer.

Reig, C., M.-D. Cubells-Beltran, D. Ramirez, S. Cardoso, and P.P. Freitas. 2008. Electrical isolators based on tunneling magnetoresistance technology. *IEEE Transactions on Magnetics* 44 (11): 4011–14.

Reig, C., M.-D. Cubells-Beltran, and D. Ramírez Muñoz. 2009. Magnetic field sensors based on giant magnetoresistance (GMR) technology: Applications in electrical current sensing. *Sensors (Basel, Switzerland)* 9 (10): 7919–42.

Reig, C., D. Ramirez, H. H. Li, and P. P. Freitas. 2005. Low-current sensing with specular spin valve structures. *IEE Proceedings: Circuits, Devices and Systems* 152 (4): 307–11.

Reig, C., D. Ramírez, F. Silva, J. Bernardo, P. Freitas, D. Ramírez, F. Silva, J. Bernardo, and P. Freitas. 2004. Design, fabrication, and analysis of a spin-valve based current sensor. *Sensors and Actuators, A: Physical* 115: 259–66.

Renhart, W., M. Bellina, C. Magele, and A. Köstinger. 2011. Hidden metallic object localization by using giant magnetic resistor sensors. *COMPEL: The International Journal for Computation and Mathematics in Electrical and Electronic Engineering* 30 (6): 1927–37.

Ripka, P., and M. Janosek. 2010. Advances in magnetic field sensors. *IEEE Sensors Journal* 10 (6): 1108–16.

Ripka, P., M. Tondra, J. Stokes, and R. Beech. 1999. AC-driven AMR and GMR magnetoresistors. *Sensors and Actuators A: Physical* 76 (1–3): 225–30.

Roldán, A., C. Reig, M. D. Cubells-Beltrán, J. B. Roldán, D. Ramírez, S. Cardoso, and P. P. Freitas. 2010a. Analytical compact modeling of GMR based current sensors: Application to power measurement at the IC level. *Solid-State Electronics* 54 (12): 1606–12.

Roldán, A., C. Reig, M. D. D. Cubells-Beltrán, J. B. B. Roldán, D. Ramírez, S. Cardoso, and P. P. P. Freitas. 2010b. Analytical compact modeling of GMR based current sensors: Application to power measurement at the IC level. *Solid-State Electronics* 54 (12): 1606–12.

Sanchez, J., D. Ramirez, S. I. Ravelo, A. Lopes, S. Cardoso, R. Ferreira, and P. P. Freitas. 2012. Electrical characterization of a magnetic tunnel junction current sensor for industrial applications. *IEEE Transactions on Magnetics* 48 (11): 2823–26.

Sánchez Moreno, J., D. Ramírez Muñoz, S. Cardoso, S. Casans Berga, A. E. Navarro Antón, and P. J. Peixeiro de Freitas. 2011. A non-invasive thermal drift compensation technique applied to a spin-valve magnetoresistive current sensor. *Sensors (Basel, Switzerland)* 11 (3): 2447–58.

Sebastia, J. P., J. Alberola Lluch, J. R. Lajara Vizcaino, and J. Santiso Bellon. 2009. Vibration detector based on GMR sensors. *IEEE Transactions on Instrumentation and Measurement* 58 (3): 707–12.

Shoshi, A., J. Schotter, P. Schroeder, M. Milnera, P. Ertl, V. Charwat, M. Purtscher, et al. 2012. Magnetoresistive-based real-time cell phagocytosis monitoring. *Biosensors & Bioelectronics* 36 (1): 116–22.

Singh, R. P., and A. M. Khambadkone. 2008. Giant magneto resistive (GMR) effect based current sensing technique for low voltage/high current voltage regulator modules. *IEEE Transactions on Power Electronics* 23 (2): 915–25.

Singh, R. P., and A. M. Khambadkone. 2014. A giant magneto resistive (GMR) effect based current sensor with a toroidal magnetic core as flux concentrator and closed-loop configuration. *IEEE Transactions on Applied Superconductivity* 24 (3): 1–5.

Stutzke, N. A., S. E. Russek, D. P. Pappas, and M. Tondra. 2005. Low-frequency noise measurements on commercial magnetoresistive magnetic field sensors. *Journal of Applied Physics* 97 (10): 10Q107.

Tamburrino, A., L. Udpa, and S. S. Udpa. 2010. Pulsed eddy-current based giant magnetoresistive system for the inspection of aircraft structures. *IEEE Transactions on Magnetics* 46 (3): 910–17.

Thompson, S. M. 2008. The discovery, development and future of GMR: The Nobel Prize 2007. *Journal of Physics D: Applied Physics* 41 (9): 093001.

Tian, G. Y., A. Al-Qubaa, and J. Wilson. 2012. Design of an electromagnetic imaging system for weapon detection based on GMR sensor arrays. *Sensors and Actuators A: Physical* 174 (February): 75–84.

Vieth, M., W. Clemens, H. van den Berg, G. Rupp, J. Wecker, and M. Kroeker. 2000. Contactless current detection with GMR sensors based on an artificial antiferromagnet (AAF) subsystem. *Sensors and Actuators A: Physical* 81 (1–3): 44–48.

Vopalensky, M., and A. Platil. 2013. Temperature drift of offset and sensitivity in full-bridge magnetoresistive sensors. *IEEE Transactions on Magnetics* 49 (1): 136–39.

Vopálenský, M., P. Ripka, J. Kubík, and M. Tondra. 2004. Improved GMR sensor biasing design. *Sensors and Actuators A: Physical* 110 (1–3): 254–58.

Wang, W., Y. Wang, L. Tu, Y. Feng, T. Klein, and J.-P. Wang. 2014. Magnetoresistive performance and comparison of supermagnetic nanoparticles on giant magnetoresistive sensor-based detection system. *Scientific Reports* 4 (January): 5716.

Wang, W., Y. Wang, L. Tu, T. Klein, Y. Feng, and J.-P. Wang. 2013. Surface modification for protein and DNA immobilization onto GMR biosensor. *IEEE Transactions on Magnetics* 49 (1): 296–99.

Yamada, S., K. Chomsuwan, Y. Fukuda, M. Iwahara, H. Wakiwaka, and S. Shoji. 2004. Eddy-current testing probe with spin-valve type GMR sensor for printed circuit board inspection. *IEEE Transactions on Magnetics* 40 (4): 2676–78.

Zeng, Z., Y. Deng, X. Liu, L. Udpa, S. S. Udpa, B. E. C. Koltenbah, R. H. Bossi, and G. Steffes. 2011. EC-GMR data analysis for inspection of multilayer airframe structures. *IEEE Transactions on Magnetics* 47 (12): 4745–52.

Zhi, X., M. Deng, H. Yang, G. Gao, K. Wang, H. Fu, Y. Zhang, D. Chen, and D. Cui. 2014. A novel HBV genotypes detecting system combined with microfluidic chip, loop-mediated isothermal amplification and GMR sensors. *Biosensors & Bioelectronics* 54 (April): 372–77.

Ziegler, S., R. C. Woodward, H. Ho-Ching Iu, and L. J. Borle. 2009. Current sensing techniques: A review. *IEEE Sensors Journal* 9 (4): 354–76.

Ziese, M., and M. J. Thornton. 2001. *Spin Electronics*. *Lecture Notes in Physics*. Berlin: Springer-Verlag.